AN ADVANCED NODAL DISCRETIZATION FOR THE QUASI-DIFFUSION LOW-ORDER EQUATIONS

Razvan Nes and Todd S. Palmer
Department of Nuclear Engineering and Radiation Health Physics
Oregon State University
116 Radiation Center
Corvallis, OR 97331-5902
nesr@engr.orst.edu; palmerts@ne.orst.edu

ABSTRACT

The quasi-diffusion method was originally developed as a rapidly-convergent iterative technique for solving transport equations. In this method, the scattering source used in a given transport sweep is obtained from the solution of the quasi-diffusion low-order (QDLO) equations. The paper presents an advanced nodal discretization of the QDLO equations for global reactor core calculations. The advantage of quasi-diffusion is that it is able to capture transport effects at the surface between unlike fuel assemblies (i.e. MOX-UO_2) better than the diffusion approximation. We discretize QDLO equations with the advanced nodal methodology described by Palmtag for diffusion. The fast flux expansion consists of polynomial functions, while the thermal flux is expanded in a combination of polynomial and hyperbolic functions. The hyperbolic expansion functions proposed by Palmtag are the analytic solutions of the zero-source diffusion equation for the thermal flux. The specific form of the QDLO equations requires the derivation of new hyperbolic basis functions which are different from those proposed by Palmtag for diffusion. We have developed a discretization of the QDLO equations with node-averaged quantities, solving the 2-D equations using the weighted residual method. These node-averaged data are assumed known from single assembly transport calculations. We have written a code in "Mathematica" that solves k-eigenvalue problems in 2-D Cartesian coordinates. The nodal quasi-diffusion low-order equations are solved numerically for several diffusion test problems, and realistic "transport" problems. The results demonstrate the validity of the method.

1. INTRODUCTION

Two-group nodal diffusion approximations are an integral part of the present generation of reactor analysis simulation tools. They are currently used to calculate full-core eigenvalues (core multiplication factors) and power distributions. An important potential weakness of the current methodology is the inaccuracy of the diffusion approximation at interfaces between significantly different fuel assemblies. Much of the "transport character" of the problem is contained within the transport-generated assembly-averaged cross-section sets; however, while core eigenvalues and assembly average powers may be accurately predicted, pin power reconstruction is often substantially less accurate. This weakness may be overcome by using the quasi-diffusion transport formalism. Here, transport equations are solved to compute "functionals" of the angular flux (Eddington tensors, boundary conditions, etc.) and this data is then used in the solution of low-order diffusion-like equations. One important advantage of this technique is that, if the data used in the low-order

equations comes from the correct transport solution, the solution of the low-order equations will be the transport scalar flux and current. In this case, full-core calculations capture transport effects to an arbitrary degree of precision[1]. The goal of this work is to develop a sophisticated nodal differencing scheme for the solution of the quasi-diffusion low-order (QDLO) equations. We have adapted the advanced nodal methodology developed by Palmtag[2] for the two-group diffusion equations with MOX and UO_2 fuel assemblies to the QDLO equations. We solve several sets of test problems and present their results to illustrate the behavior of this method.

2. THE QUASIDIFFUSION EQUATIONS

The quasi-diffusion (QD) method was developed in 1964 by Gol'din[3] as a non-linear method of solving the linear Boltzmann equation. QD methods are rapidly convergent transport algorithms which use functionals of the angular flux (i.e. Eddington tensors and boundary information) computed from transport sweeps in diffusion-like calculations of the scalar flux, which in turn are the source of particles in the next transport sweep. QD methods generate discrete transport solutions that are influenced by both the discretizations of the transport and the low-order diffusion-like operator. The low-order operator contains transport corrections, thus the QD-accelerated solution does not, in general, converge to the unaccelerated transport solution[4].

Consider the general-geometry k-eigenvalue transport equation for monoenergetic neutrons with isotropic scattering

$$\hat{\Omega}\cdot\nabla\psi(\hat{r},\hat{\Omega})+\Sigma(\hat{r})\psi(\hat{r},\hat{\Omega})=\frac{1}{4\pi}\Sigma_s(\hat{r})\Phi(\hat{r})+\frac{1}{4\pi k}\upsilon\Sigma_f(\hat{r})\Phi(\hat{r}) \tag{1}$$

where

- $\hat{\Omega}$ is the direction,
- $\psi(\hat{r},\hat{\Omega})$ is the angular flux,
- $\Sigma(\hat{r})$ is the total cross section,
- $\Sigma_s(\hat{r})$ is the scattering cross section,
- $\Phi(\hat{r})$ is the scalar flux,
- k is the multiplication factor,
- υ is the number of neutrons per fission, and
- $\Sigma_f(\hat{r})$ is the fission cross section.

Integrating each term of Eq. (1) over all directions, yields[5]

$$\nabla\cdot J(\hat{r})+\Sigma_r(\hat{r})\Phi(\hat{r})=\frac{1}{k}\upsilon\Sigma_f(\hat{r})\Phi(\hat{r}), \tag{2}$$

where we used the definition of the scalar flux $\Phi(\hat{r})$,

$$\Phi(\hat{r})=\int_{4\pi}\psi(\hat{r},\hat{\Omega})d\Omega. \tag{3}$$

In Eq. (2), $\Sigma_r(\hat{r})$ represents the removal cross-section, defined as

$$\Sigma_r(\hat{r})=\Sigma(\hat{r})-\Sigma_s(\hat{r}). \tag{4}$$

Multiplying Eq. (1) by Ω_x, Ω_y, and Ω_z, and integrating over all directions yields

$$J_i(\hat{r}) = -\frac{1}{\Sigma(\hat{r})}\nabla(E_{ij}(\hat{r})\Phi(\hat{r})) \qquad \text{i,j=x,y,z .} \tag{5}$$

In Eq. (5) $J_i(\hat{r})$ are the projections of the neutron current in each of the three dimensions and $E_{ij}(\hat{r})$ are the components of the symmetric, positive-defined Eddington tensor:

$$E_{ij}(\hat{r}) = \frac{4\pi \int_{4\pi} \Omega_i \Omega_j \psi(\hat{r},\hat{\Omega}) d\Omega}{\int_{4\pi} \psi(\hat{r},\hat{\Omega}) d\Omega} \qquad \text{i,j=x,y,z .} \tag{6}$$

Equations (2) and (5) are known as the quasi-diffusion low-order (QDLO) equations. Eq. (2) is simply a balance equation and Eq. (5) is an exact definition of the transport current, which has a form similar to Fick's law.

If we consider two neutron energy groups (1=fast neutrons, 2=thermal neutrons) the QDLO equations become

$$\nabla\ J_1(\hat{r}) + \Sigma_{r1}(\hat{r})\Phi_1(\hat{r}) = \frac{1}{k}(\upsilon\Sigma_{f1}(\hat{r})\Phi_1(\hat{r}) + \upsilon\Sigma_{f2}(\hat{r})\Phi_2(\hat{r})) \tag{7}$$

$$\nabla\ J_2(\hat{r}) + \Sigma_{r2}(\hat{r})\Phi_2(\hat{r}) = \Sigma_{12}(\hat{r})\Phi_1(\hat{r}) , \tag{8}$$

and

$$J_{gi}(\hat{r}) = -\frac{1}{\Sigma_g(\hat{r})}\nabla(E_{gij}(\hat{r})\Phi_g(\hat{r})) , \tag{9}$$

where

$$E_{gij}(\hat{r}) = \frac{4\pi \int_{4\pi} \Omega_i \Omega_j \psi_g(\hat{r},\hat{\Omega}) d\Omega}{\int_{4\pi} \psi_g(\hat{r},\hat{\Omega}) d\Omega} \qquad \text{for i,j=x,y,z and g=1,2 .} \tag{10}$$

In deriving Eqs. (7) and (8) we assumed that the only source of thermal neutrons consists of fast neutrons slowing down from group 1 to group 2 and no upscattering occurs.

3. ADVANCED NODAL DISCRETIZATION

The problem domain is the $x-y$ plane divided into non-overlapping square regions (nodes) of dimension h. Non-dimensional coordinates (u,v) are introduced, and Figure 1 illustrates these for a square node that occupies the position (i, j) in a regular array.

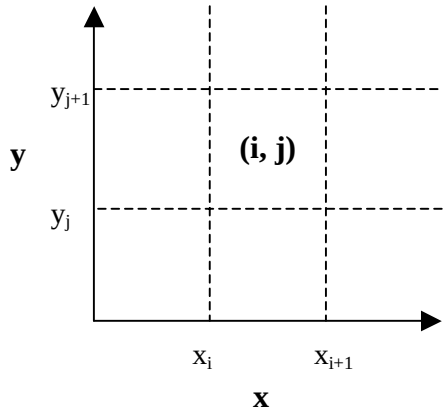

Figure 1. 2-D representation of a square node located at position x_i, y_j

Based on the geometry of the problem, the coordinates (u,v) are defined by

$$u = \frac{2x - x_{i+1} - x_i}{2h}, \tag{12}$$

and

$$v = \frac{2y - y_{i+1} - y_i}{2h}. \tag{13}$$

Using these coordinates, assuming constant cross-sections and Eddington tensor components, and inserting the neutron currents given by Eq. (9) into Eqs. (7) and (8), the balance equations become

$$\begin{aligned} &-\frac{1}{h^2}\left(\frac{E_{1xx}}{\Sigma_1}\frac{\partial^2\Phi_1(u,v)}{\partial u^2} + \frac{E_{1xy}}{\Sigma_1}\frac{\partial^2\Phi_1(u,v)}{\partial u\partial v} + \right. \\ &\left. + \frac{E_{1yx}}{\Sigma_1}\frac{\partial^2\Phi_1(u,v)}{\partial v\partial u} + \frac{E_{1yy}}{\Sigma_1}\frac{\partial^2\Phi_1(u,v)}{\partial v^2}\right) + \Sigma_{r1}\Phi_1(u,v) = \\ &= \frac{1}{k}\left(\upsilon\Sigma_{f1}\Phi_1(u,v) + \upsilon\Sigma_{f2}\Phi_2(u,v)\right) \end{aligned} \tag{14}$$

and

$$\begin{aligned} &-\frac{1}{h^2}\left(\frac{E_{2xx}}{\Sigma_2}\frac{\partial^2\Phi_2(u,v)}{\partial u^2} + \frac{E_{2xy}}{\Sigma_2}\frac{\partial^2\Phi_2(u,v)}{\partial u\partial v} + \frac{E_{2yx}}{\Sigma_2}\frac{\partial^2\Phi_2(u,v)}{\partial v\partial u} + \right. \\ &\left. + \frac{E_{2yy}}{\Sigma_2}\frac{\partial^2\Phi_2(u,v)}{\partial v^2}\right) + \Sigma_{r2}\Phi_2(u,v) = \Sigma_{12}\Phi_1(u,v). \end{aligned} \tag{15}$$

The method used to spatially discretize equations (14) and (15) is the method of weighted residuals (MWR).The fast flux in the interior of each node is approximated by a 2-D, non-separable expansion of polynomial functions:

$$\Phi_1(u,v) = \sum_{m=0}^{4}\sum_{n=0}^{4} a_{mn} f_m(u) f_n(v). \tag{16}$$

The functions f_m are polynomial basis functions of the form

$$
\begin{aligned}
f_0(\xi) &= 1, \\
f_1(\xi) &= \xi, \\
f_2(\xi) &= 3\xi^2 - \frac{1}{4}, \\
f_3(\xi) &= 4\xi(\xi + \frac{1}{2})(\xi - \frac{1}{2}), \\
f_4(\xi) &= (\xi^2 - \frac{1}{20})(\xi + \frac{1}{2})(\xi - \frac{1}{2}).
\end{aligned}
\tag{17}
$$

The thermal flux is approximated by a 2-D, non-separable, expansion of polynomial and hyperbolic functions

$$\Phi_2(u,v) = \sum_{m=0}^{4}\sum_{n=0}^{4} b_{mn} f_m(u) f_n(v) + \sum_{l=1}^{8} c_l g_l(u,v). \tag{18}$$

In Eqs. (16) and (18) only 15 of 25 a_{mn} coefficients and 19 of 25 b_{mn} coefficients are non-zero.

The basis functions used in (18) are

$$
\begin{aligned}
g_1(u,v) &= \cosh(\gamma_1 u), \\
g_2(u,v) &= \sinh(\gamma_1 u), \\
g_3(u,v) &= \cosh(\gamma_2 v), \\
g_4(u,v) &= \sinh(\gamma_2 v), \\
g_5(u,v) &= \cosh(\gamma_3 (v - \vartheta_1 u)/\sqrt{2}), \\
g_6(u,v) &= \sinh(\gamma_3 (v - \vartheta_1 u)/\sqrt{2}), \\
g_7(u,v) &= \cosh(\gamma_3 (v - \vartheta_2 u)/\sqrt{2}), \\
g_8(u,v) &= \sinh(\gamma_3 (v - \vartheta_2 u)/\sqrt{2}),
\end{aligned}
\tag{19}
$$

with

$$
\begin{aligned}
\gamma_1 &= \sqrt{\frac{h^2 \Sigma_{r2} \Sigma_2}{E_{2xx}}}, \\
\gamma_2 &= \sqrt{\frac{h^2 \Sigma_{r2} \Sigma_2}{E_{2yy}}}, \\
\gamma_3 &= \sqrt{\frac{h^2 \Sigma_{r2} \Sigma_2 E_{2xx}}{E_{2xx} E_{2yy} - E_{2xy}{}^2}}, \\
\theta_1 &= \frac{E_{2xy} + \sqrt{-E_{2xy}{}^2 + E_{2xx} E_{2yy}}}{E_{2xx}}, \\
\theta_2 &= \frac{E_{2xy} - \sqrt{-E_{2xy}{}^2 + E_{2xx} E_{2yy}}}{E_{2xx}}.
\end{aligned}
\tag{20}
$$

These functions are exact (analytic) solutions of the zero-source thermal neutrons balance equation [Eq. (15)].

The weighted residual method requires a set of weight functions; which we choose to be low-order polynomials:

$$\begin{aligned} w_0(u,v) &= 1, \\ w_1(u,v) &= f_1(u), \\ w_2(u,v) &= f_1(v), \\ w_3(u,v) &= 144\, f_1(u)\, f_1(v), \\ w_4(u,v) &= 4\, f_2(u), \\ w_5(u,v) &= 4\, f_2(v), \\ w_6(u,v) &= 16\, f_2(u)\, f_2(v). \end{aligned} \tag{21}$$

We define the *n*-th weighted moment of a function $R(u,v)$ by

$$< w_n(u,v), R(u,v) >= \int_{-\frac{1}{2}}^{+\frac{1}{2}} \int_{-\frac{1}{2}}^{+\frac{1}{2}} R(u,v) w_n(u,v) du dv \,. \tag{22}$$

The zero-th weighted moment of the fast and thermal neutron fluxes represent node-averaged quantities. The average fast flux is thus $\overline{\overline{\Phi}}_1 = a_{00}$ and the average thermal flux is given by

$$\begin{aligned} \overline{\overline{\Phi}}_2 &= b_{00} + \frac{2}{\gamma_1} c_1 \sinh(\frac{\gamma_1}{2}) + \frac{2}{\gamma_2} c_3 \sinh(\frac{\gamma_2}{2}) + \\ &+ \frac{8}{\gamma_3^{\,2}\theta_1} c_5 \sinh(\frac{\gamma_3}{2\sqrt{2}}) \sinh(\frac{\gamma_3\theta_1}{2\sqrt{2}}) + \frac{8}{\gamma_3^{\,2}\theta_2} c_7 \sinh(\frac{\gamma_3}{2\sqrt{2}}) \sinh(\frac{\gamma_3\theta_2}{2\sqrt{2}}). \end{aligned} \tag{23}$$

In order to solve the Quasi-Diffusion Low Order Equations by the MWR, 23 equations for 23 coefficients are needed for each node of the problem. The 23 equations are generated from the following conditions:

- 7 weighted residual moments in the fast group
- 4 surface-averaged continuity conditions in the fast group
- 4 surface-averaged continuity conditions in the thermal group
- 4 corner conditions in the fast group
- 4 corner conditions in the thermal group.

The 19 thermal polynomial expansion coefficients are expressed in terms of the 15 fast flux expansion coefficients based on fact that the hyperbolic basis functions [Eq. (19)] are analytic solutions of the zero-source thermal neutron balance equations with spatially constant components of the Eddington tensor and cross-sections.

The matrix problem is solved, iteratively, for expansion coefficients and k-eigenvalue by the method of Power iteration[6]. All the calculations are performed by a code written in Mathematica[7].

4. RESULTS

The QDLO equations are solved for several diffusion test problems (diagonal Eddington tensor with diagonal entries equal to 1/3), and "transport" problems (Eddington tensor with diagonal entries different from one-third and zero or positive off-diagonal components). In the transport problems, the Eddington functionals are chosen to be within the range of values representative of two-node UO_2-MOX fuel assembly transport calculations.

The method provides accurate solutions (multiplication factor k and thermal to fast flux ratio) for one-node, constant cross-section and Eddington tensor component problems, with zero-flux or zero-current boundary conditions.

The two-node problems assume a UO_2-fueled assembly next to a MOX-fueled assembly[2]. This configuration is chosen because UO_2 and MOX have significantly different neutronic properties, so UO_2/MOX systems are excellent for investigating the behavior of neutron fluxes at the surface between unlike assemblies. Zero current boundary conditions are applied to the boundaries of the configurations, as shown in Figure 2.

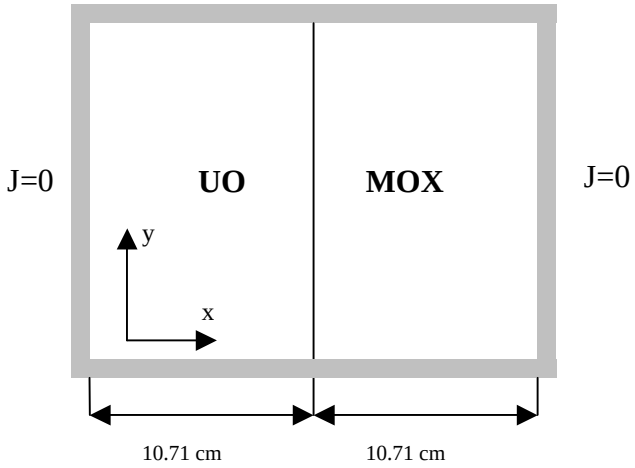

Figure 2. UO_2-MOX configuration

Various configurations are obtained by using UO_2 and MOX fuels of various enrichments in ^{235}U and Pu, respectively.

Table 1 shows the multiplication factor, UO_2 assembly power and their relative errors from QDLO calculations using the two-group, single assembly cross sections from Table 2. Columns 5 and 6 show the relative errors from the advanced nodal diffusion methodology calculations presented by Palmtag[2]. These sets of computations are compared to CASMO-4 14-group results[2] which are reproduced here in columns 8 and 9. In Table 1 U_x and M_y stand for x %-enriched UO_2 and y %-enriched MOX.

Table 1. Two-node UO_2-MOX assembly, multiplication factor and power calculations

Config.	k	N	Relative error k (%)	UO_2 assembly power	Relative error (%) UO_2 power
0	1	2	3	4	5
U_3/U_4	1.29121	18	6.2×10^{-3}	0.93167	0.74
U_4/U_5	1.34542	18	2.2×10^{-3}	0.93569	2.3
U_3/U_5	1.31531	18	8.4×10^{-3}	0.88585	1.2
U_3/M_8	1.20273	20	1.2	0.94333	1.2
U_3/M_{12}	1.20885	21	1.6	0.90974	1.2
U_4/M_8	1.23828	20	0.8	1.01375	2.0
U_4/M_{12}	1.24387	21	1.2	0.98002	2.0
U_5/M_8	1.26385	20	0.52	1.06130	2.3
U_5/M_{12}	1.37004	20	7.0	1.06350	5.9

Table 1, continued. Two-node UO_2-MOX assembly, multiplication factor and power calculations

Config.	Relative error of k (%) [2]	Relative error of UO_2 power (%)[2]	Reference k	Reference UO_2 power
0	6	7	8	9
U_3/U_4	2.4×10^{-2}	0.69	1.29113	0.9386
U_4/U_5	1.0×10^{-2}	0.43	1.34545	0.9580
U_3/U_5	6.3×10^{-2}	1.11	1.31520	0.8969
U_3/M_8	0.239	0.87	1.21721	0.9312
U_3/M_{12}	0.306	0.69	1.22896	0.8986
U_4/M_8	0.346	1.64	1.24830	0.994
U_4/M_{12}	0.405	1.47	1.25888	0.9611
U_5/M_8	0.435	2.12	1.27035	1.0372
U_5/M_{12}	0.487	1.96	1.28014	1.0042

Table 2. Two-group single assembly cross sections

Property	Assembly type					
	UO_2 3%	UO_2 4%	UO_2 5%	MOX 4%	MOX 8%	MOX 12%
Σ_1	0.286867	0.286714	0.204091	0.286466	0.285875	0.285233
Σ_2	0.97970	0.980551	0.987944	1.07985	1.16774	1.23263
Σ_{12}	0.016756	0.016229	0.015738	0.013630	0.011853	0.010644
Σ_{a1}	0.009530	0.010234	0.010895	0.012956	0.015327	0.017049
Σ_{a2}	0.082606	0.098603	0.113317	0.197823	0.290164	0.350338
$\upsilon\Sigma_{f1}$	0.006758	0.008092	0.009357	0.008436	0.012259	0.015427
$\upsilon\Sigma_{f2}$	0.129545	0.163555	0.194709	0.321278	0.483443	0.587795
$k_{\inf}$	1.256776	1.323053	1.366686	1.149925	1.177585	1.201939

The fast and thermal neutron flux shapes for the UO_2 (3%)-MOX (12%) configuration are presented in Figure 3 and Figure 4, respectively. In both figures, the UO_2 fuel assembly is the closest to the viewer. The fast flux is higher in the MOX assembly, due to its higher fission cross-sections. The steepest variation is observed near the surface between the two assemblies, smoothing out as the reflecting boundaries are approached. The smallest errors occur for the case of two UO_2 assemblies.

The thermal flux varies strongly at the surface between nodes mainly due to Σ_{a2}, which is higher in the UO_2 assembly than in the MOX assembly. Better results are obtained if, instead of two-group single-assembly cross-sections, 14-group cross-sections are collapsed to two-group with the actual spectrum[2].

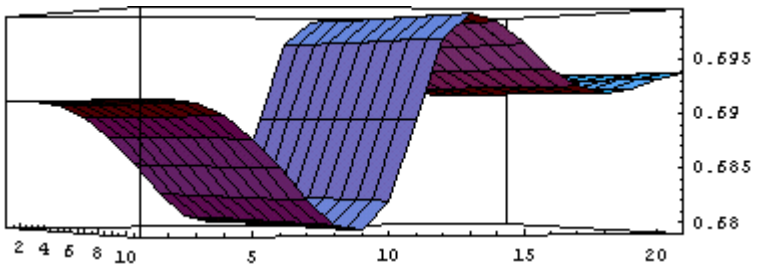

Figure 3. Fast neutron flux in UO_2 (3%)-MOX (12%) configuration

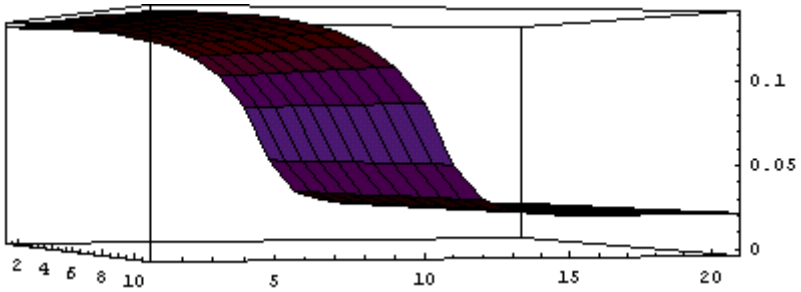

Figure 4. Thermal neutron flux in UO_2 (3%)-MOX (12%) configuration

In the multiple-node problems, the k-eigenvalues and power distributions are calculated for configurations of UO_2 (UX), MOX (PX), and water (R) presented in Figure 5.

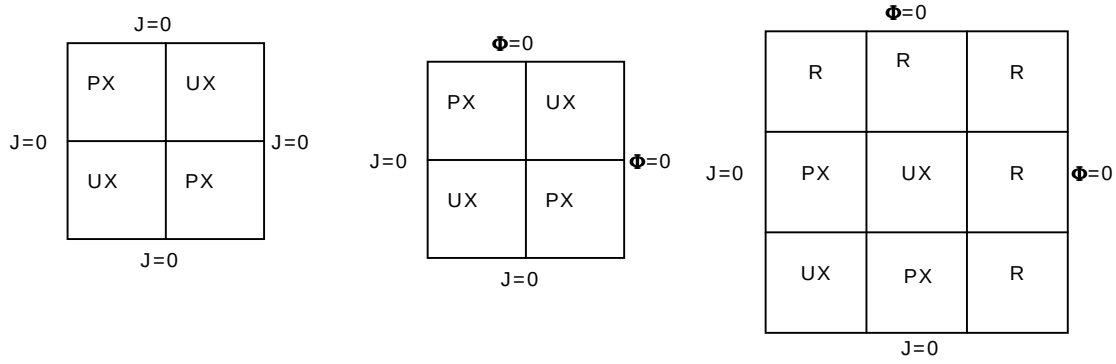

Figure 5. UO_2-MOX (C1, C2) and UO_2-MOX-water (C3) configurations

Cross-section data for these problems come from single assembly NEACRP benchmark calculations (zero-current boundary conditions)[2], and are presented in Table 3. Results from QDLO calculations of these problems are shown in Table 4, columns 2 through 4. The relative errors, columns 5 through 7, are calculated with respect to reference k-eigenvalues and normalized assembly powers presented

in Table 5[2] The reference solution (Table 5) for each configuration is a 2-D, 2-group, heterogeneous static diffusion calculation performed using one node per fuel pin[2].

Table 3. Assembly homogenization results for NEACRP benchmark

Homogenized parameter	**Assembly type**	
	UX	**PX**
$k_{\inf}$	0.998181	1.026669
Σ_1	0.277778	0.277778
Σ_2	0.833333	0.833333
Σ_{a1}	0.009226	0.013791
Σ_{a2}	0.092663	0.231691
$\upsilon\Sigma_{f1}$	0.004570	0.006852
$\upsilon\Sigma_{f2}$	0.113537	0.344583
Σ_{21}	0.020430	0.015864

Table 4. NEACRP benchmark, homogenized node calculations

Config.	**N**	**k**	**Assembly Power**		**Error (%)**		
			UX	**PX**	**k**	**UX**	**PX**
0	**1**	**2**	**3**	**4**	**5**	**6**	**7**
C_1	60	1.01974	0.87346	1.1265	$5.6\text{x}10^{-2}$	0.14	0.11
C_2	40	0.91245	1.02145	0.97855	0.62	0.69	0.66
C_3	48	0.940336	0.90558	1.09442	0.24	1.2	1.0

Table 5. NEACRP benchmark, homogenized node calculations, reference values

Config.	**Reference values [2]**		
	k	**UX**	**PX**
0	**7**	**8**	**9**
C_1	1.01914	0.8747	1.1253
C_2	0.90685	1.0282	0.9718
C_3	0.93806	0.9165	1.0835

Compared to STENCIL[2] the QDLO results from Table 4 are less accurate in reproducing the reference values, Table 5. Palmtag[2] shows also the results produced by other methods (CONQUEST, SIMULATE-3, and PANTHER). QDLO yields results comparable to these for assembly powers, still producing less accurate results for the k-eigenvalues.

In the QD problem with realistic Eddington tensor components we consider a 4-node domain with semi-reflecting boundaries as shown in Figure 6. Each node corresponds to a fuel assembly, all assemblies being identical.

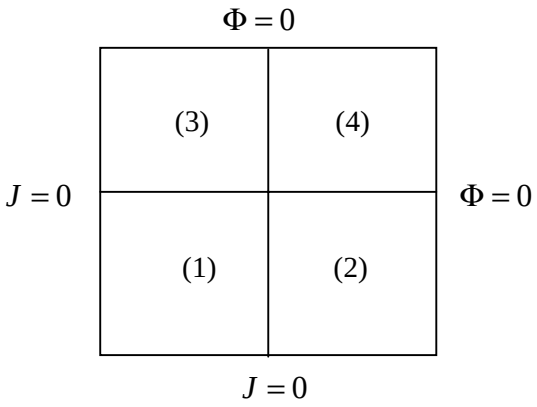

Figure 6. Semi-reflecting boundaries, four-node problem

The multiplication factor k of this configuration by using the nodal QDLO methodology for $E^{ij}_{g,xx} = E^{ij}_{g,yy}$ from 0.30 to 0.36 and $E^{ij}_{g,xy} = E^{ij}_{g,yx}$ from 0.0 to 0.04. Cross-sections are the ones in Table 3, for PX assemblies. The results show that k decreases when Eddington functionals increase. This behavior is due to increased leakage, directly related to bigger functional values. The calculated values for k and the dependence of k on **E** are shown in Table 6 and Figure 7.

Table 6. Calculated multiplication factors for various Eddington functionals

$E^{ij}_{g,xy}$	$E^{ij}_{g,xx} = E^{ij}_{g,yy}$			
	0.30	0.32	0.34	0.36
0.00	0.928595	0.922699	0.916875	0.911121
0.01	0.927200	0.921318	0.915508	0.909769
0.02	0.925912	0.920036	0.914233	0.908502
0.03	0.924729	0.918852	0.913050	0.907321
0.04	0.923653	0.917766	0.911958	0.906225

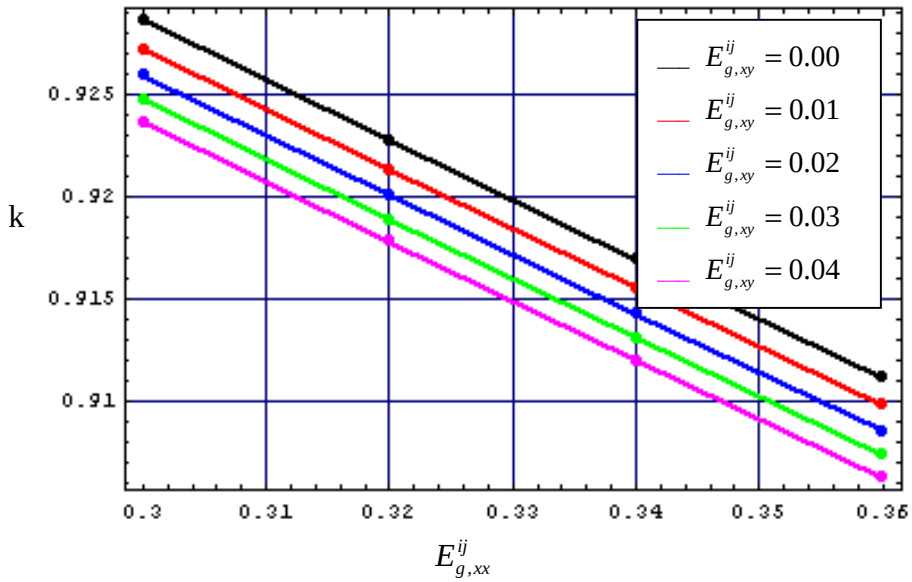

Figure 7. Multiplication factor versus diagonal components at various values of off-diagonal components of Eddington tensor

Increased off-diagonal Eddington tensor components also affect the power distribution between nodes by enhancing the flow of neutrons towards certain nodes. For example in our problem the power in node 4 increases with increasing $E^{ij}_{g,xy}$, while power in nodes 1, 2 and 3 decreases. Table 7 summarizes these results, showing the variation of node-averaged power (P) and its relative rate of variation $\left(\frac{1}{P}\frac{dP}{dE^{ij}_{g,xy}} \right)$.

Table 7. The effect of off-diagonal Eddington tensor components on the power distribution

$E^{ij}_{g,xy}$	**Node 1**		**Node 2, 3**		**Node 4**	
	P	$\frac{1}{P}\frac{dP}{dE^{ij}_{g,xy}}$	P	$\frac{1}{P}\frac{dP}{dE^{ij}_{g,xy}}$	P	$\frac{1}{P}\frac{dP}{dE^{ij}_{g,xy}}$
0.00	4.99998	-0.323	2.07107	-0.140	8.57873	2.55
0.01	4.98446	-0.299	2.06789	-0.167	8.79730	2.48
0.02	4.97020	-0.274	2.06415	-0.194	9.01471	2.40
0.03	4.95719	-0.250	2.05984	-0.224	9.23107	2.34
0.04	4.94544	-0.225	2.05494	-0.253	9.44652	2.28

In Figure 8 node averaged power is plotted against off-diagonal Eddington functionals.

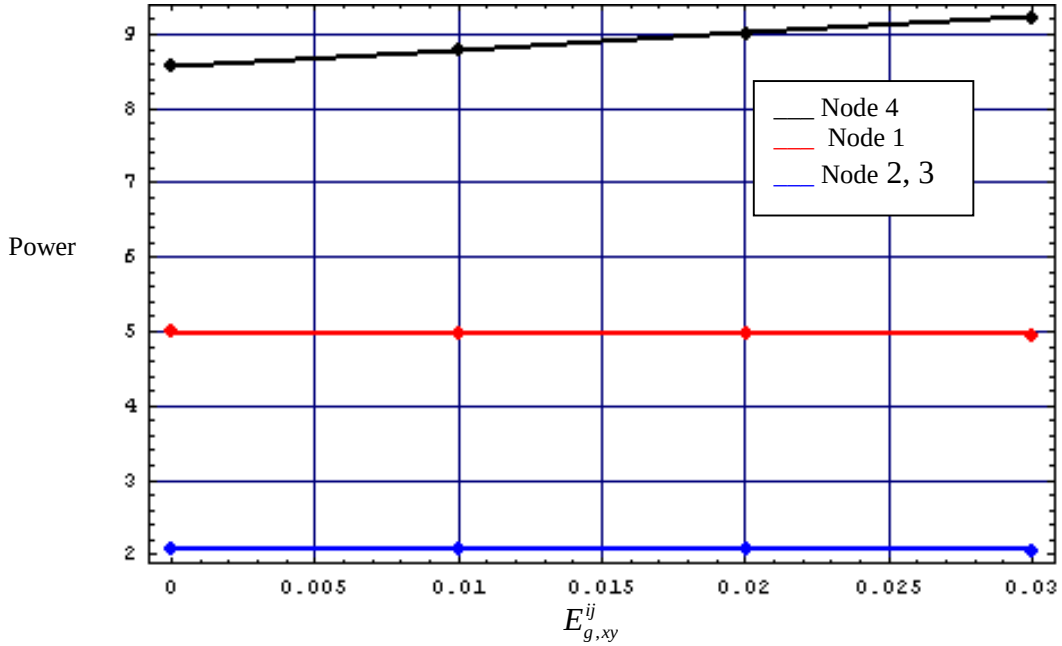

Figure 8. Node-averaged power versus off-diagonal Eddington tensor elements

5. CONCLUSIONS

Two-group nodal diffusion approximations, along with single-assembly transport-generated cross section sets are currently used to calculate full-core eigenvalues (core multiplication factors) and power distribution. The inaccuracy of the diffusion approximation at interfaces between significantly different fuel assemblies can be overcome by using the quasi-diffusion transport formalism. Here, transport equations are solved to compute "functionals" of the angular flux (Eddington tensors, boundary conditions, etc.) and this data is then used in the solution of low-order diffusion-like equations. One important advantage of this technique is that, if the data used in the low-order equations comes from the correct transport solution, the solution of the low-order equations will be the transport scalar flux and current. In this case full-core calculations are capturing transport effects to an arbitrary degree of precision. We have adapted the advanced nodal methodology developed by Palmtag[2] for the two-group, 2-D diffusion equations with MOX and UO_2 fuel assemblies to the QDLO equations in Cartesian coordinates.

A discretization of the QDLO equations with constant nodal cross-sections and Eddington tensors was developed. The two-dimensional QDLO equations are solved by the weighted residual method, with non-separable polynomial and hyperbolic basis functions expansions of the fast and thermal neutron fluxes. The hyperbolic basis functions of the thermal flux expansion are different from those used with the diffusion equation[2]. To form a set of equations which, when solved, will yield the flux expansion coefficients, several conditions are imposed: weighted moment equations, flux and current continuity, node balance and boundary conditions. This yields 23 equations for 23 flux expansion coefficients for each node of the problem. To perform these calculations we developed a code, written in "Mathematica", which allows us to generate matrices for multiple-node problems, solve for flux expansion coefficients, and k-eigenvalues. A number of diffusion test problems (Eddington tensor with diagonal entries equal to 1/3, and zero-off-diagonal entries), and "transport" problems (Eddington tensor with diagonal entries different from one-third and zero or positive off-diagonal components) are solved. In the transport problems, the Eddington functionals are chosen to be within the range of values representative for two-node UO_2-MOX fuel assembly transport calculations. The results show that, for fuel assemblies characterized by "diffusive" data ($E_{xx} = E_{yy} = 1/3$, $E_{xy} = E_{yx} = 0$), the QDLO nodal discretization limits to the nodal diffusion discretization derived by Palmtag[2].

While the QDLO calculations performed on one-node, zero-current, boundary condition diffusion problems and two-node, zero-current boundary condition problems with UO_2-UO_2 assemblies are in excellent agreement with the benchmark and analytic solutions, UO_2-MOX configurations show more important discrepancies that are due to the single-assembly homogenized cross-sections used in the calculations. Compared to other authors' results, four- and nine-node problems show similar power distribution discrepancies. Multiple-node k-eigenvalue problems exhibit larger discrepancies, but these can be diminished by using adjusted diffusion coefficients[2]. The results of the "transport" problems demonstrate the influence of Eddington functionals on homogenized flux and on the multiplication factor k.

The assumption of constant nodal data is a significant limitation of this work. Transport codes, however, can provide with great accuracy the flux profile and, subsequently, space-dependent values for the homogenized cross-sections and the components of the Eddington tensor. An accurate reproduction of fine mesh transport results requires the incorporation of both higher spatial moments of the cross-sections and assembly-surface Eddington tensor data.

Future work will address these limitations by incorporating space-dependent assembly Eddington tensor and cross-sections in a FORTRAN code that will perform flux and k-eigenvalue calculations. We will also extend the methodology based on QDLO equations, developing a 3-D reactor core model. An efficient algorithm for the solution system of the linear system of equations will be incorporated into the FORTRAN code. Future work will also include a comparison between the nodal solution of QDLO equations, with and without discontinuity factors, and the fine mesh transport calculation results.

ACKNOWLEDGEMENTS

The authors wish to thank Dmitriy Anistratov for his analytic solution of the zero-source, constant nodal data LOQD equations, and Marvin Adams and Kord Smith for helpful discussions. This work was supported by Nuclear Energy Research Initiative (NERI) Program of the US Department of Energy under grant No. DE-FG03-99SF21922.

REFERENCES

1. D.Y. Anistratov, M.L. Adams, T.S. Palmer, K.S. Smith, "An Innovative Reactor Analysis Methodology Based on a Quasidiffusion Nodal Core Model", *DOE NERI Proposal* (1999).

2. S.Palmtag, "Advanced Nodal Methods for MOX Fuel Analysis", PhD Thesis, MIT (1997)

3. V.Ya. Goldin, "A Quasi-Difussion Method of Solving the Kinetic Equation ", *USSR Comp. Math. and Math. Phys.*, **4**, pp.136-149 (1967)

4. Adams, M.L. and Larsen, E.W., "Fast Iterative Methods for Discrete Ordinates Particle Transport Calculations", *Progress in Nuclear Energy*, **40**, No.1, pp 3-159 (2002)

5. M.M. Miften, E.W.Larsen, "A Symmetrized Quasidiffusion Method for Solving Transport Problems in Multidimensional Geometries", *Joint International Conference on Mathematical Methods and Supercomputing in Nuclear Applications*, Karlsruhe, 19-23 April, Germany, Vol.1,pp. 702-711 (1993)

6. Rade, L. and Westergren, B., "*Beta Mathematics Handbook*", CRC Press, Boca Raton US (1992)

7. S.Wolfram, "*Mathematica, A System for Doing Mathematics by Computer*", Second Edition, Addison-Wesley (1991)